Voxel shift and Interpolation for Hadamard-encoded MR images.

L. Fleysher[1], R. Fleysher[1], S. Liu[1], and O. Gonen[1]
[1]Department of Radiology, NYU School of Medicine, New York, NY, United States

INTRODUCTION. Gradient (Fourier) and radio-frequency (RF) phase encodings are two established localization methods for both MRI (1,2) and MR spectroscopic imaging (MRSI) (3,4,5,6). Voxel shift and interpolation operations available for Fourier encoding are especially attractive for MRSI since they allow to arbitrary align the relatively coarse imaging grid with specific anatomical regions within the field-of-view (FOV) in post-processing. Despite mathematical similarities between the gradient and RF localizatoin methods, absence of interpolation and voxel-shift analogs for the latter placed it at a disadvantage. We address these issues by developing the theory of voxel shift and interpolation for Hadamard encoding.

THEORY. The spin-density $\rho(x)$ at any point x is related to the complex digitized signal a_p from the MR receiver by Equation [1], where P is the number of the encoding steps and $\phi_p(x)$ are the Hadamard functions (see Fig.1) defined on the field of view L. The reconstructed image I_n in the voxel n is simply the average spin-density over the voxel size $\Delta=L/P$ (see Equation [2]). As a simple consequence, it is clear that to construct an image I_m^s interpolated to voxel size δ and shifted by s with respect to the original image it is enough to change the range of the integration in the Equation [2] (see Equation [3]).

$$\rho(x)=\sum_{p=-P/2}^{P/2-1} a_p\phi_p(x) \qquad [1]$$

$$I_n=\frac{1}{\Delta}\int_{n\Delta}^{(n+1)\Delta}\rho(x)dx=\frac{1}{\Delta}\sum_{p=-P/2}^{P/2-1}a_p\int_{n\Delta}^{(n+1)\Delta}\phi_p(x)dx \qquad [2]$$

$$I_m^s=\frac{1}{\delta}\int_{m\delta-s}^{(m+1)\delta-s}\rho(x)dx=\frac{1}{\delta}\sum_{p=-P/2}^{P/2-1}a_p\int_{m\delta-s}^{(m+1)\delta-s}\phi_p(x)dx \qquad [3]$$

METHODS. To assess the effectiveness of the shift/interpolation operations, a four-compartment cylindrical phantom (see Fig.2) was built. Each compartment is a cylinder with internal diameter of 121mm and 11.5mm thickness with 1.0mm walls between the compartments and represents a distinct voxel in 1D if viewed along the phantom's axis. To enable observation of voxel bleeds and other reconstruction artifacts the compartments were "labeled" by filling them with 100mM (protons) chemical solutions with distinct singlet resonance frequencies (Methanol, 3.4ppm; Na-acetate, 1.9ppm; tert-buthanol, 1.2ppm; Na-3-Methyl-Silyl propionate, 0ppm) and performing spectroscopic imaging. Due to the one-to-one correspondence between frequencies and compartments, spectral line intensity at a specific frequency reveals the magnitude of an artifact. The water signal, at 4.7ppm, was suppressed during the acquisition with WET (7) and removed during post-processing (8). All experiments were performed in a 3T Magnetom Trio clinical MRI scanner (Siemens AG, Erlangen, Germany) equipped with a TEM transmit-receive head coil (TEM3000, MRInstruments, Minneapolis, MN). Our custom CSI-based auto-shim procedure yielded a 6Hz water linewidth from the whole phantom allowing clean separation of the partition "labels" (the singlets). A parallelepiped volume-of-interest (VOI) of 12.5x12.5x50mm^3 was excited with TE=35ms and TR=1600ms PRESS. The long aspect of the VOI was oriented along the phantom axis and was placed to contain all four phantom partitions exactly. Data sampling with 1024 complex points at 500us per point were used. The MRSI data were processed off-line using our custom reconstruction software.

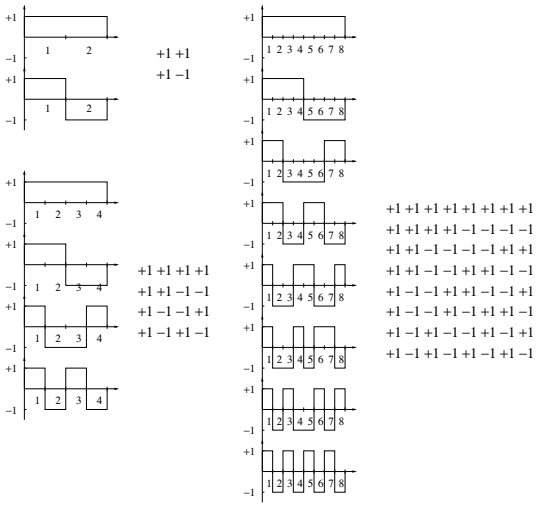

Fig.1 *Hadamard functions (solid lines) and Hadamard matrices for P=2,4 and 8.*

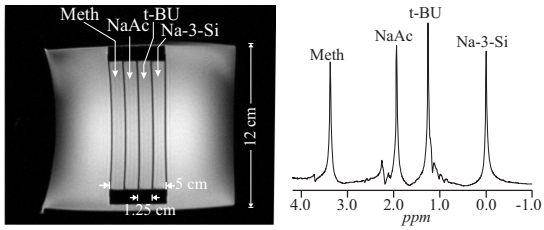

Fig.2 *Sagittal section of the phantom (left) and the absolute 3T spectrum from the phantom (right).*

RESULTS. The reconstructed data before and after voxel shift/interpolation operations are presented in Fig.3. The panel **a** of the figure presents the data as acquired, while panel **b** depicts the shifted image, hence each but the edge voxel in it contain two spectral lines. Interpolated and shifted-interpolated spectroscopic images are shown in panels **c** and **d**. As expected, since panels **c** and **d** contain higher resolution images of panels **a** and **b**, respectively, each voxel in the former contains only one (correct) spectral line.

CONCLUSION. We have introduced the interpolation and voxel-shift operations for Hadamard encoded imaging and shown their equivalence to the well known analogs for Fourier encoding. This formalism reduces the disparity between these two complementary methodologies and aids in providing more choice in matching a localization method to a specific problem at hand.

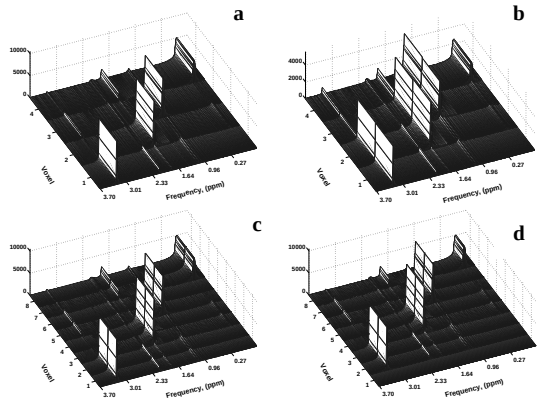

Fig.3 *The ^{1}H NMR spectra with reconstructed voxels: (**a**) aligned with the phantom partitions; (**b**) shifted by half the partition size; (**c**) interpolated to half partition size; (**d**) shifted by half the partition size and interpolated.*

References. [1] Edelstein WA, Hutchison JM, Johnson G, Redpath T. Phys Med Biol (1980);25:751-756. [2] Maudsley AA. Magn Reson Med (1986);3:768-777. [3] Brown TR, Kincaid BM, Ugurbil K. Proc Natl Acad Sci USA (1982);79:3523-3526. [4] Maudsley AA, Hilal SK, Perman WH, Simon HE. J Magn Reson (1983);51:147-152. [5] Bolinger L, Leigh JS. J Magn Reson (1988); 80:162-167. [6] Goelman G, Subramanian VH, Leigh JS. J Magn Reson (1990);89:437-454. [7] Ogg RJ, Kingsley PB, Taylor JS. J Magn Reson B (1994);104:1-10. [8] Marion D, Ikura M, Bax A. J Magn Reson (1989);84:425-430.